THE JOURNAL OF PHYSICAL CHEMISTRY Letters

Letter

Cite This: J. Phys. Chem. Lett. 2018, 9, 3886−3890

pubs.acs.org/JPCL

Exploiting Coordinate Scaling Relations To Accelerate Exact Exchange Calculations

Martin P. Bircher and Ursula Rothlisberger*

Laboratoire de Chimie et Biochimie Computationnelles, Ecole Polytechnique Fédérale de Lausanne, Lausanne 1015, Switzerland

Supporting Information

ABSTRACT: Exact exchange is an important constituent in many state-of-the-art approximations to the exchange-correlation (xc) functional of Kohn−Sham DFT. However, its evaluation can be computationally intensive, which can be particularly prohibitive in DFT-based molecular dynamics (MD) simulations, often restricted to semilocal functionals. We derive a scheme based on the formal coordinate scaling properties of the exact xc functional that allows for a substantial reduction of the cost of the evaluation of both the exact exchange energy and potential. We show that within a plane-wave/pseudopotential framework, excellent accuracy is retained, while speed ups from up to ∼6 can be reached. The coordinate scaling thus accelerates hybrid-functional-based first-principles MD simulations by nearly one order of magnitude.

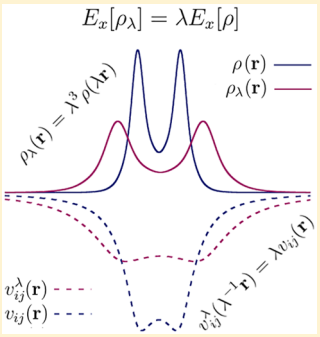

The history of Kohn−Sham density functional theory (KS-DFT)[1,2] has been marked by the quest for increasingly accurate approximations to the exchange-correlation (xc) functional. Whereas a computationally tractable form for the exact xc functional[3] remains, alas, elusive, a plethora of approximate forms have been developed and successfully applied over the past decades.[4]

Known properties of the exact xc functional have served as a valuable guide in the design of many an approximate functional,[5−7] but their use has mostly been limited to the theoretical realm of functional development[8−12] rather than the improvement of the computational performance in practical implementations. Here we show how the use of a simple scaling relation[13−15] can substantially lower the computational overhead of the evaluation of exact exchange in plane waves for isolated systems. This is achieved without loss of accuracy, enabling studies of systems that have hitherto been untractable.

Among the conditions an exact functional must fulfill, the coordinate scaling relation[9,16] for the exact exchange energy is of particular simplicity. Figure 1 illustrates the concept of density scaling on a hydrogen molecule. Given a (L^1-norm-conserving) electron density scaled in the coordinates by a constant λ

$$\rho_\lambda(\mathbf{r}) = \lambda^3 \rho(\lambda\mathbf{r}) \tag{1}$$

where $\lambda > 1$ contracts the density and $\lambda < 1$ stretches it out, the exchange energy is homogeneous to degree one

$$E_x[\rho_\lambda] = \lambda E_x[\rho] \tag{2}$$

Whereas a similar relation only gives an upper bound for the correlation energy, in the case of the exchange functional, eq 2 imposes strict boundaries on functional forms.

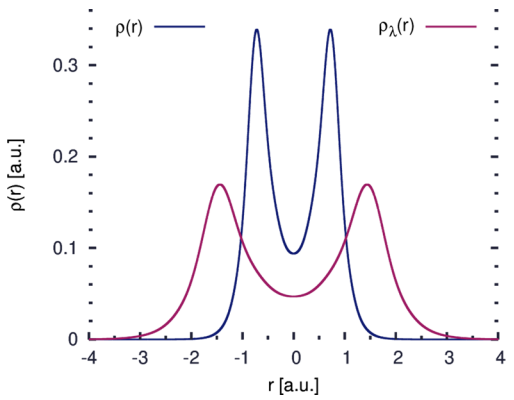

Figure 1. Illustration of the coordinate scaling at the example of the hydrogen molecule. Shown are a cut of the N-electron density $\rho(\mathbf{r})$ along the bonding axis as well as its 1D coordinate-scaled analogue $\rho_\lambda(\mathbf{r})$ for $\lambda = 0.5$.

This scaling relation is trivially derived from the exact exchange functional, the familiar functional form of which is given as the exchange energy (or Fock exchange) of the single Slater determinant of the N_b occupied Kohn−Sham orbitals that sum up to $\rho(\mathbf{r}) = \sum_i^{N_b} |\psi_i(\mathbf{r})|^2$

$$E_x[\rho] = \frac{1}{2} \sum_{ij} \iint \mathrm{d}\mathbf{r}\, \mathrm{d}\mathbf{r}' \frac{\psi_i^*(\mathbf{r})\psi_j^*(\mathbf{r}')\psi_j(\mathbf{r})\psi_i(\mathbf{r}')}{|\mathbf{r} - \mathbf{r}'|} \tag{3}$$

Equation 3 is the primordial ingredient in the family of hybrid exchange-correlation functionals[17] that combine a fraction of

Received: May 24, 2018
Accepted: June 25, 2018
Published: June 25, 2018

DOI: 10.1021/acs.jpclett.8b01620
J. Phys. Chem. Lett. 2018, 9, 3886−3890

exact exchange with semilocal functional forms and that have seen tremendous success over the last decades.[18,19] The advent of hybrid functionals extended the applicability of density functional theory (DFT) to many chemical systems for which a description at the generalized gradient approximation (GGA) level was hampered by insufficient accuracy, substantially improving properties ranging from ionization potentials over excitation energies to reaction enthalpies.[19]

The improved accuracy of energetics and excitation energies obtained from hybrid functionals is of particular appeal to first-principles ground- and excited-state molecular dynamics (MD) simulations. However, because of the large computational overhead associated with the evaluation of the integral in eq 3, applications using hybrid functionals are often limited by the time scale that can be simulated at an achievable computational cost.[20] The overhead due to the evaluation of the Fock integral can be particularly expensive in the plane-wave/pseudopotential framework that is frequently used for first-principles MD.[21]

Hybrid functionals are most commonly used within the generalized Kohn−Sham (GKS) scheme,[22] where the (local) Kohn−Sham optimized effective potential can be replaced by the familiar orbital-dependent form known from Hartree−Fock exchange. In a plane-wave basis at the Γ-point, the gradient of the exact exchange energy with respect to every one out of N_b orbital expansion coefficients $\overline{\psi}_i(\mathbf{G})$ is then obtained from a discrete Fourier transform $\mathcal{F}$[23,24]

$$\frac{\partial E_x}{\partial \overline{\psi}_i^*(\mathbf{G})} = \mathcal{F}_{D^S_{\Delta\mathbf{R}}}\left[\sum_j \psi_j(\mathbf{R}) v_{ij}(\mathbf{R})\right] \tag{4}$$

where we have introduced capital symbols (**G**,**R**) to denote discrete representations of continuous functions. The domain $D^S_{\Delta\mathbf{R}}$ of the discrete Fourier transform is the real-space mesh points **R** spaced by Δ**R** that are contained within the entire simulation supercell *S*. For notational simplicity, we have restricted $D^S_{\Delta R}$ to the 1D case

$$D^S_{\Delta R} = \{R \mid (0 \le R < l) \wedge (R = n\Delta R,\ 0 \le n < n_{\max},\ n \in \mathbb{Z}_{\ge 0})\} \tag{5}$$

where l is the edge length of the simulation supercell. A generalization to 3D Cartesian space is straightforward. For a given supercell, the spacing of the real-space grid Δ**R** and the number of grid points $n_{\max}$ is defined by the value of the cutoff energy in reciprocal space, E_{cut}. The potential $v_{ij}(\mathbf{R})$ is determined by two discrete Fourier transforms, exploiting the fact that the Coulomb operator is diagonal in reciprocal space

$$v_{ij}(\mathbf{R}) = \mathcal{F}^{-1}_{D^S_{\Delta\mathbf{R}}}[\Phi(\mathbf{G})(\mathcal{F}_{D^S_{\Delta\mathbf{R}}}[\psi_i^*(\mathbf{R})\psi_j(\mathbf{R})])] \tag{6}$$

where $\Phi(\mathbf{G})$ is an appropriately defined form of the Coulomb operator in reciprocal space **G** that eliminates the divergence at **G** = 0.[25,26] Orbital pair products can therefore be conveniently obtained in real space, whereas the associated Coulomb potential is straightforwardly computed from the diagonal reciprocal-space Coulomb operator. The computational cost for the evaluation of a given pair is only determined by the granularity of the real-space mesh; a resolution **R**′ halved in every Cartesian component with respect to a reference mesh **R** decreases the cost for every 3D fast Fourier transform (FFT) by a factor of ∼8.

Whereas for first-principles MD plane waves offer many advantages over localized, atom-centered bases (such as intrinsic periodicity, absence of Pulay forces and basis set superposition effects, and scaling as N log N due to the extensive use of fast Fourier transforms in the calculation of $\mathcal{F}$), following eqs 3, 4 and 6, practical calculations employing hybrid functionals for a system with N_b occupied KS orbitals require at least $(3N_b)^2$ additional FFTs with respect to a GGA. Although the use of blocking techniques can improve the effective scaling for large N_b on a large number of processors,[24] the computational cost can remain prohibitively expensive in the absence of specialized computational hardware that provides multiples of thousands of threads.

This problem is exacerbated in the case of isolated systems, which are usually required for nonperiodic systems in a full QM or QM/MM context. To recover the first/nearest image interaction rather than the infinitely periodic description, which is intrinsic to a plane-wave expansion, the Poisson equation has to be solved under appropriate boundary conditions. A solution to this problem has, among others, been proposed by Tuckerman and Martyna[27] (TM) using an appropriate Fourier series representation for $\Phi(\mathbf{G})$. This approach requires that the simulation supercell spans twice the range of the charge density; because the cost of an FFT scales approximately cubically $(N \text{ log } N)^3$ with respect to the supercell volume, this approach carries a significant computational overhead due to large regions of the simulation supercell where the orbitals are effectively zero. For a system under the TM decoupling scheme, we will distinguish the domain of non-negligible electron density $D^\rho_{\Delta\mathbf{R}}$ within $D^S_{\Delta\mathbf{R}}$ by the superscript ρ, and its 1D analogue reads

$$D^\rho_{\Delta R} = \{R \mid (l/4 \le R < 3l/4) \wedge (R = n\Delta R,\ n_{\max}/4 \le n < 3n_{\max}/4,\ n \in \mathbb{Z}_{\ge 0})\} \tag{7}$$

In combination with the $(3N_b)^2$ FFTs required in the calculation of the exact exchange energy, this can make calculations on isolated systems prohibitively expensive for a typical number of electronic states N_b that would still be tractable in an infinitely periodic system.

In the following, based on the extension of the coordinate scaling relations to the Kohn−Sham orbitals,[16,28] we shall demonstrate that the exact exchange energy and potential for isolated systems described by a plane-wave expansion of the GKS orbitals can be straightforwardly obtained from the coordinate-scaled quantities at a substantially lower computational cost.

The homogeneous coordinate scaling of the density by λ can be generalized to the KS orbitals according to[28]

$$\psi_i^\lambda(\mathbf{r}) = \lambda^{3/2}\psi_i(\lambda\mathbf{r}) \tag{8}$$

where $\lambda^{3/2}$ ensures that the norm of the N-electron density be conserved. The corresponding Coulomb potential $v_{ij}^\lambda(\mathbf{r})$ due to a scaled orbital pair $\psi_i^{\lambda*}(\mathbf{r})\psi_j^\lambda(\mathbf{r})$ expressed in terms of the unscaled Kohn−Sham orbitals reads

$$v_{ij}^\lambda(\mathbf{r}) = \int d\mathbf{r}' \frac{\psi_j^{\lambda*}(\mathbf{r}')\psi_i^\lambda(\mathbf{r}')}{|\mathbf{r}-\mathbf{r}'|} = \int d\mathbf{r}' \frac{\lambda^3\psi_j^*(\lambda\mathbf{r}')\psi_i(\lambda\mathbf{r}')}{|\mathbf{r}-\mathbf{r}'|} \tag{9}$$

Introducing the coordinate transformation $\mathbf{q} = \lambda\mathbf{r}$, where the infinitesimal volume element changes according to the Jacobian of the transformation matrix, $d\mathbf{r} = \lambda^{-3}\, d\mathbf{q}$, one finds

DOI: 10.1021/acs.jpclett.8b01620
J. Phys. Chem. Lett. 2018, 9, 3886−3890

Table 1. Total Energy, HOMO−LUMO Gap $\Delta\epsilon^{\mathrm{LUMO}}_{\mathrm{HOMO}}$, and Singlet Excitation Energies for the Organic Dye DMABN Obtained from the Standard $v_{ij}(\mathbf{r})$ and Its Scaled Counterpart Presented in This Work (eq 14; $\lambda = 0.5$)[a]

	E_{tot} (a.u.)	$\Delta\epsilon^{\mathrm{LUMO}}_{\mathrm{HOMO}}$ (eV)	S_1 (eV)	S_2 (eV)	S_3 (eV)	S_4 (eV)	S_5 (eV)
full $v_{ij}(\mathbf{r})$	−76.689581	4.7690	4.410	4.465	4.752	4.992	5.080
scaled $v_{ij}(\mathbf{r})$	−76.689586	4.7588	4.408	4.504	4.753	5.080	5.140
difference	5.0×10^{-6}	0.0002	0.002	0.039	0.001	0.088	0.060

[a]Calculations were carried out in an orthorhombic 37.5 × 18.75 × 18.75 Å^3 supercell at a plane-wave cutoff of 75 Ry using the B3LYP[17,30] xc functional.

$$v_{ij}^{\lambda}(\lambda^{-1}\mathbf{q}) = \lambda \int \mathrm{d}\mathbf{q}' \frac{\psi_j^*(\mathbf{q}')\psi_i(\mathbf{q}')}{|\mathbf{q}-\mathbf{q}'|} \tag{10}$$

By comparing with the Coulomb potential $v_{ij}(\mathbf{r})$ of an unscaled orbital pair $\psi_i^*(\mathbf{r})\psi_j(\mathbf{r})$, it follows that the coordinate scaled Coulomb potential and its unscaled counterpart are related according to

$$v_{ij}^{\lambda}(\lambda^{-1}\mathbf{r}) = \lambda v_{ij}(\mathbf{r}) \tag{11}$$

Whereas the Kohn−Sham $\psi_i^{\lambda}(\mathbf{r})$ minimize T_s for a given scaled density, no such proof exists for orbitals obtained from a GKS-type potential. In GKS theory, the $\psi_i^{\lambda}(\mathbf{r})$ are therefore not necessarily the minimizing orbitals associated with $\rho_{\lambda}(\mathbf{r})$. By extending eqs 9−11 to the exact energy functional, it is readily seen that any set of orbitals obtained from eq 8 obeys a relation of the type $E_x[\{\psi^{\lambda}\}] = \lambda E_x[\{\psi\}]$, independent of it coming from the minimizing determinant of $\rho_{\lambda}(\mathbf{r})$. Because here the Euler−Lagrange equation is solved on the initial, unscaled orbital space of $\psi_i(\mathbf{r})$, the $\psi_i^{\lambda}(\mathbf{r})$ of GKS theory are not constrained to be the minimizing orbitals for a given $\rho_{\lambda}(\mathbf{r})$. Instead, they can be defined to be the set of orbitals that fulfill eq 2, which allows for the same scaling relations to be applied to both GKS and KS orbitals. T_s itself is always calculated using the original, unscaled orbitals.

We now seek to lower the resolution of the real-space grid $\mathbf{R}$ for the discrete Fourier transforms in eq 6 without loss of accuracy. This is possible by exploiting the considerable volume in the supercell where the density is zero, which is imposed by the necessity for a decoupling of the Poisson equation.

We set $\lambda = 0.5$ and define the set of stretched, coordinate-scaled Kohn−Sham orbitals

$$\psi_i^{\lambda}(\mathbf{R}') = \lambda^{3/2}\psi_i(\lambda\mathbf{R}' + \mathbf{T}_D(\lambda)) \tag{12}$$

where the translation $\mathbf{T}_D(\lambda) = \frac{1}{2}(\mathbf{l} - \lambda\mathbf{l})$ ensures that the orbitals remain centered within the periodic supercell of length $\mathbf{l}$, thus preserving translational invariance. Because the representation of $\psi_i(\mathbf{R})$ is not continuous, the coordinates $\mathbf{R}'$ obtained from eq 12 have to be discretized on a grid with $\Delta\mathbf{R}' = 2\Delta\mathbf{R}$. Only the nonzero domain $D^{\rho}_{\Delta\mathbf{R}}$ of the unscaled orbitals is now used in constructing $\psi_i^{\lambda}(\mathbf{R}')$. The spatial extent of the simulation supercell remains the same. The resulting coordinate-scaled Kohn−Sham orbitals are now defined on the domain $D^{S}_{\Delta\mathbf{R}'}$ containing the points of a coarser mesh $\mathbf{R}'$ on the entire supercell S. For the 1D case

$$D^{S}_{\Delta R'} = \{R' \,|\, (0 \le R' < l) \wedge (R' = m\Delta R', \; 0 \le m < \lambda n_{\max}, \; m \in \mathbb{Z}_{\ge 0})\} \tag{13}$$

$v_{ij}^{\lambda}(\mathbf{R}')$ is then easily obtained from eq 6 by performing two discrete Fourier transforms on the domain $D^{S}_{\Delta\mathbf{R}'}$, $v_{ij}^{\lambda}(\mathbf{R}') = \mathcal{F}^{-1}_{D^{S}_{\Delta\mathbf{R}'}}\{\Phi(\mathbf{G})[\mathcal{F}_{D^{S}_{\Delta\mathbf{R}'}}(\psi_i^{\lambda *}(\mathbf{R}')\psi_j^{\lambda}(\mathbf{R}'))]\}$, which reduces the energy cutoff in $\mathbf{G}$ by a factor of 8 compared with the one used for $v_{ij}(\mathbf{R})$. On the basis of eq 11, one obtains $v_{ij}(\mathbf{R})$ from the low-resolution, scaled Coulomb potential $v_{ij}^{\lambda}(\mathbf{R}')$ according to

$$v_{ij}(\mathbf{R}) = \begin{cases} \lambda^{-1} v_{ij}^{\lambda}(\lambda^{-1}\mathbf{R} + \mathbf{T}_D(\lambda^{-1})) & \text{for} \quad \mathbf{R} \in D^{\rho}_{\Delta\mathbf{R}} \\ 0 & \text{for} \quad \mathbf{R} \in D^{S}_{\Delta\mathbf{R}} \setminus D^{\rho}_{\Delta\mathbf{R}} \end{cases} \tag{14}$$

where $\mathbf{T}_D(\lambda^{-1})$ again ensures proper centring of $v_{ij}(\mathbf{R})$ within the periodic supercell. After multiplication by $\psi_j(\mathbf{R})$, $v_{ij}(\mathbf{R})$ can be used to update the expansion coefficients $\overline{\psi}_i(\mathbf{G})$ via eq 4 from the full $v_{ij}(\mathbf{R})$, which is again defined for all points of $D^{S}_{\Delta\mathbf{R}}$. We have implemented this approach in the CPMD code.[29]

Table 1 compares total energy, HOMO−LUMO gaps, and the first five excited states obtained from the standard $v_{ij}(\mathbf{r})$ to those obtained from eq 14 illustrated by the example of the organic dye DMABN. Total energies between the approaches differ by only 0.3×10^{-4} kcal/mol. The forces on the atoms span a range from 10^{-2} to 10^{-5} a.u. and differ at maximum by 1%. However, 80% of the deviations are <0.1%. The HOMO−LUMO gap is identical within 2×10^{-4} eV, and good accuracy is retained in the excitation energies for the first five singlet states, where the maximum deviation is observed for the S_4 state. Still, the difference between the approaches is <0.1 eV, that is, <2%. The differences are not sensitive to changes in the geometry that are smaller than the grid spacing (cf. Supporting Information).

Practically, the performance of the algorithm described here is limited not only by the last Fourier transform in eq 4, which is carried out on the full reference mesh, but also by interprocessor communication in a distributed memory framework. Table 2 compares execution times for the calculation of the first five excited states of both DMABN and a DMABN trimer illustrated by the example of the three different routines in which the exact exchange contribution has to be calculated: ODIIS[31] wave function optimization to obtain the occupied (but nondiagonal) ground-state KS orbitals, the Davidson diagonalization that yields the canonical (occupied and nonoccupied) KS orbitals, and the final Davidson diagonalization of the TD-DFT matrix. In the CPMD code, the fast index of the 3D real-space mesh, x, is distributed over MPI tasks.[24] To resolve load-balancing issues, a second parallelization layer is available, where electronic states are distributed over processor groups. All timings are given for the most efficient parallel setup (x planes versus bands) for a given number of CPU cores, such that they are representative of practical applications.

For a single DMABN molecule ($N_b = 28$), an average step of DIIS optimization is sped up by a factor of about $\eta = 2.5$, whereas the calculation of the orbital eigenvalues (diagonaliza-

DOI: 10.1021/acs.jpclett.8b01620
J. Phys. Chem. Lett. 2018, 9, 3886−3890

Table 2. Execution Time for Optimization (ODIIS) and Diagonalization (Davidson) of the Ground-State KS Wavefunction as Well as the Diagonalization of the TDDFT Matrix (LR) for Both a Monomer and a Trimer of DMABN (28 and 84 occupied states, respectively)[a]

	DMABN			$(DMABN)_3$		
	t_{ref} (s)	t_{λ} (s)	η	t_{ref} (s)	t_{λ} (s)	η
ODIIS	3.94	1.59	2.50	34.28	7.62	4.50
Davidson	13.63	3.02	4.52	110.00	22.08	4.98
LR	85.00	25.43	3.34	976.30	170.22	5.74

[a]Values averaged over 10 iterations are given for both the full $v_{ij}(\mathbf{r})$ (ref) and its scaled counterpart (λ) and have been used to calculate the speed up η. Calculations were carried out in an orthorhombic 25.0 × 12.5 × 12.5 Å^3 supercell at a plane-wave cutoff of 75 Ry using the B3LYP[17,30] xc functional on 256 CPU cores. Optimal parallel configurations are compared. The values for the full $v_{ij}(\mathbf{r})$ were obtained by using four CP groups and a block size of 4 in the calculation of the exact exchange. The calculations using the scaled $v_{ij}(\mathbf{r})$ were carried out using four CP groups and a block size of 14. For details of the parallelization, see ref 24.

tion of the noncanonical KS orbitals) is accelerated by about η = 4.5. The solution of the Tamm−Dancoff equation for the five first singlet states is η = 3.3 times faster when using the scaled densities. Speed ups are particularly sizable for a DMABN trimer (N_b = 84), where an average DIIS step is accelerated by a factor of η = 4.5. The speed up of η = 4.9 in the calculation of the canonical KS orbitals remains comparable to the monomer, whereas the diagonalization of the TD-DFT matrix is faster by a factor of η = 5.7. These considerable speed ups make the density scaling approach particularly beneficial for applications where many independent trajectories have to be gathered in parallel, such as thermodynamic integration or excited-state applications like surface hopping, thus making optimal use of the computing resources available.

Here we have shown how the simple coordinate-scaling relations of Kohn−Sham DFT can be applied in practical calculations, offering a substantial performance benefit over conventional approaches. The calculation of the orbital-pair Coulomb potential on the scaled orbitals allows for a much lower cutoff energy in the discrete Fourier transforms, thereby significantly reducing the computational cost. Sizeable speed ups can be achieved, and the coordinate-scaled calculation of exact exchange can increase the available time scale or the number of independent trajectories that can be run within a given time by a factor of up to ∼6, which significantly increases both sampling accuracy and efficiency with respect to current state-of-the-art plane-wave/pseudopotential calculations.

■ ASSOCIATED CONTENT

Supporting Information

The Supporting Information is available free of charge on the ACS Publications website at DOI: 10.1021/acs.jpclett.8b01620.

Table of the response of the approach to a change in geometry smaller than the grid spacing $\Delta\mathbf{R}$ (PDF)

■ AUTHOR INFORMATION

Corresponding Author

*E-mail: ursula.roethlisberger@epfl.ch.

ORCID

Martin P. Bircher: 0000-0002-6905-3130

Ursula Rothlisberger: 0000-0002-1704-8591

Notes

The authors declare no competing financial interest.

■ ACKNOWLEDGMENTS

M.P.B. is indebted to Simone Meloni for all of the fruitful discussions on plane-wave algorithms and exact exchange approximations. U.R. gratefully acknowledges financial support from the Swiss National Science Foundation Grant No. 200020-146645 and the NCCR MUST.

■ REFERENCES

(1) Hohenberg, P.; Kohn, W. Inhomogeneous Electron Gas. *Phys. Rev.* **1964**, *136*, B864−B871.

(2) Kohn, W.; Sham, L. J. Self-Consistent Equations Including Exchange and Correlation Effects. *Phys. Rev.* **1965**, *140*, A1133−A1138.

(3) Lieb, E. H. Density functionals for coulomb systems. *Int. J. Quantum Chem.* **1983**, *24*, 243−277.

(4) Burke, K. Perspective on density functional theory. *J. Chem. Phys.* **2012**, *136*, 150901.

(5) Perdew, J. P.; Ruzsinszky, A.; Sun, J.; Burke, K. Gedanken densities and exact constraints in density functional theory. *J. Chem. Phys.* **2014**, *140*, 18A533.

(6) Levy, M. In *Density Functional Theory of Many-Fermion Systems*; Löwdin, P.-O., Ed.; Advances in Quantum Chemistry; Academic Press: 1990; Vol. *21*, pp 69−95.

(7) Levy, M. In *Density Functional Theory*; Gross, E. K. U., Dreizler, R. M., Eds.; Springer US: Boston, MA, 1995; pp 11−31.

(8) Levy, M.; Ou-Yang, H. Nonuniform coordinate scaling requirements for exchange-correlation energy. *Phys. Rev. A: At., Mol., Opt. Phys.* **1990**, *42*, 651−652.

(9) Borgoo, A.; Teale, A. M.; Tozer, D. J. Effective homogeneity of the exchange-correlation and non-interacting kinetic energy functionals under density scaling. *J. Chem. Phys.* **2012**, *136*, 034101.

(10) Borgoo, A.; Teale, A. M.; Tozer, D. J. Revisiting the density scaling of the non-interacting kinetic energy. *Phys. Chem. Chem. Phys.* **2014**, *16*, 14578−14583.

(11) Gledhill, J. D.; Tozer, D. J. System-dependent exchange-correlation functional with exact asymptotic potential and $\epsilon_{HOMO}\approx -I$. *J. Chem. Phys.* **2015**, *143*, 024104.

(12) Sharpe, D. J.; Levy, M.; Tozer, D. J. Approximating the Shifted Hartree-Exchange-Correlation Potential in Direct Energy Kohn-Sham Theory. *J. Chem. Theory Comput.* **2018**, *14*, 684−692.

(13) Sham, L. J. Local Exchange Approximations and the Virial Theorem. *Phys. Rev. A: At., Mol., Opt. Phys.* **1970**, *1*, 969−970.

(14) Levy, M.; Perdew, J. P. Hellmann-Feynman, virial, and scaling requisites for the exact universal density functionals. Shape of the correlation potential and diamagnetic susceptibility for atoms. *Phys. Rev. A: At., Mol., Opt. Phys.* **1985**, *32*, 2010−2021.

(15) Liu, S.; Parr, R. G. Expansions of the correlation-energy density functional $E_c[\rho]$ and its kinetic-energy component $T_c[\rho]$ in terms of homogeneous functionals. *Phys. Rev. A: At., Mol., Opt. Phys.* **1996**, *53*, 2211−2219.

(16) Calderín, L. Generalization of homogeneous coordinate scaling in density-functional theory. *Phys. Rev. A: At., Mol., Opt. Phys.* **2012**, *86*, 032510.

(17) Becke, A. D. A new mixing of Hartree-Fock and local density-functional theories. *J. Chem. Phys.* **1993**, *98*, 1372−1377.

(18) Csonka, G. I.; Perdew, J. P.; Ruzsinszky, A. Global Hybrid Functionals: A Look at the Engine under the Hood. *J. Chem. Theory Comput.* **2010**, *6*, 3688−3703.

(19) Mardirossian, N.; Head-Gordon, M. Thirty years of density functional theory in computational chemistry: an overview and

DOI: 10.1021/acs.jpclett.8b01620
J. Phys. Chem. Lett. 2018, 9, 3886−3890

extensive assessment of 200 density functionals. *Mol. Phys.* **2017**, *115*, 2315−2372.
(20) Liberatore, E.; Meli, R.; Rothlisberger, U. A Versatile Multiple Time Step Scheme for Efficient ab Initio Molecular Dynamics Simulations. *J. Chem. Theory Comput.* **2018**, *14*, 2834.
(21) Chawla, S.; Voth, G. A. Exact exchange in ab initio molecular dynamics: An efficient plane-wave based algorithm. *J. Chem. Phys.* **1998**, *108*, 4697−4700.
(22) Seidl, A.; Görling, A.; Vogl, P.; Majewski, J. A.; Levy, M. Generalized Kohn-Sham schemes and the band-gap problem. *Phys. Rev. B: Condens. Matter Mater. Phys.* **1996**, *53*, 3764−3774.
(23) Wu, X.; Selloni, A.; Car, R. Order-*N* implementation of exact exchange in extended insulating systems. *Phys. Rev. B: Condens. Matter Mater. Phys.* **2009**, *79*, 085102.
(24) Weber, V.; Bekas, C.; Laino, T.; Curioni, A.; Bertsch, A.; Futral, S. Shedding Light on Lithium/Air Batteries Using Millions of Threads on the BG/Q Supercomputer. In *2014 IEEE 28th International Parallel and Distributed Processing Symposium*; IEEE: 2014; pp 735−744.
(25) Gygi, F.; Baldereschi, A. Self-consistent Hartree-Fock and screened-exchange calculations in solids: Application to silicon. *Phys. Rev. B: Condens. Matter Mater. Phys.* **1986**, *34*, 4405−4408.
(26) Broqvist, P.; Alkauskas, A.; Pasquarello, A. Hybrid-functional calculations with plane-wave basis sets: Effect of singularity correction on total energies, energy eigenvalues, and defect energy levels. *Phys. Rev. B: Condens. Matter Mater. Phys.* **2009**, *80*, 085114.
(27) Martyna, G. J.; Tuckerman, M. E. A reciprocal space based method for treating long range interactions in ab initio and force-field-based calculations in clusters. *J. Chem. Phys.* **1999**, *110*, 2810−2821.
(28) Parr, R.; Weitao, Y. *Density-Functional Theory of Atoms and Molecules*; International Series of Monographs on Chemistry; Oxford University Press, 1994.
(29) www.cpmd.org, CPMD. Copyright IBM Corp 1990−2008, Copyright MPI für Festkörperforschung Stuttgart 1997−2001.
(30) Stephens, P. J.; Devlin, F. J.; Chabalowski, C. F.; Frisch, M. J. Ab Initio Calculation of Vibrational Absorption and Circular Dichroism Spectra Using Density Functional Force Fields. *J. Phys. Chem.* **1994**, *98*, 11623−11627.
(31) Hutter, J.; Lüthi, H. P.; Parrinello, M. Electronic structure optimization in plane-wave-based density functional calculations by direct inversion in the iterative subspace. *Comput. Mater. Sci.* **1994**, *2*, 244−248.

DOI: 10.1021/acs.jpclett.8b01620
J. Phys. Chem. Lett. 2018, 9, 3886−3890